*G. H. Aronson* [1] *and R. O. Ritchie* [2]

# Optimization of the Electrical Potential Technique for Crack Growth Monitoring in Compact Test Pieces Using Finite Element Analysis

**ABSTRACT:** Finite element procedures are used to optimize the efficiency of the electrical potential technique for monitoring the initiation and slow growth of cracks, as applied to the compact tension fracture test piece. An analysis of various configurations of current input and potential measurement lead placement is performed to optimize the accuracy, sensitivity, and reproducibility of measurement and to maximize output voltages. Numerical calibration curves are computed for selected configurations and are confirmed by experimental measurements.

**KEY WORDS:** crack propagation, fractures (materials), fatigue (materials), electrical potential method, finite element analysis

Over the past 10 to 15 years, the electrical potential, or potential drop, technique [1] has gained increasingly wide acceptance in fracture research as one of the most accurate and efficient methods for monitoring the initiation and propagation of cracks. The method was first employed over 30 years ago in Germany [2] and applied to flaw detection in large structures [3]. However, Barnett and Troiano [4] first used the technique for laboratory research in a study of hydrogen-induced brittle fracture in notched tensile specimens. Subsequent early development then occurred concurrently in Sweden [5], England [6], and the United States [7-12]. The technique has now been successfully applied for a wide range of fracture problems, such as the measurement of velocities of fast running cleavage cracks [5]; for detection of crack initiation in toughness [7,8,11-13] and fatigue tests [14]; for determination of slow crack growth rates under conditions of sustained loading [15], fatigue [16-18], stress corrosion [18-20], hydrogen embrittlement [4,18-20], and creep [21]; and for evaluation of the extent of crack closure in fatigue crack propagation studies [22].

The method relies on the fact that there will be a disturbance in the electrical potential field about any discontinuity in a current-carrying body, the magnitude of the disturbance depending directly on the size and shape of the discontinuity. For the application of crack growth monitoring, the method entails passing a constant current (maintained constant by external means) through a cracked test specimen and measuring the change in electrical potential across the crack as it propagates. With increasing crack length, the uncracked cross-sectional area of the test piece decreases, its electrical resistance increases, and thus the potential difference between two points spanning the crack rises. By monitoring this potential increase $V_a$, and comparing it with some reference potential $V_0$, the crack length-to-width ratio $a/W$ may be determined through the use of the relevant calibration curve for the particular test piece geometry concerned.

In practice, calibration curves are generally given in the form of $V_a/V_{a0}$ versus $a/W$, where $V_a$ is the potential drop across the crack length $a$ and $V_{a0}$ is the reference potential drop across the initial starter notch (or crack) of length $a_0$. Through the use of such nondimensionalized ratios, calibration curves become independent of material properties, test piece thickness, and magnitude of input current (provided it remains constant) and are mainly a function of specimen and crack geometry and the locations of current input and potential measurement leads.

For a given configuration, calibration of the method involves finding solutions to Laplace's equation within the boundary conditions of a particular test piece geometry, where, for a strip of metal of constant thickness, containing a transverse crack, the steady state electrical potential at coordinate $x,y$ is given by

$$\nabla^2 V = 0 \tag{1}$$

assuming that the current $I$ flows only in the plane of the strip (that is, in the $x$-$y$ plane).

Solutions to Eq 1 can be derived in a number of ways, both experimentally and theoretically. In many instances, experimental calibrations have been achieved by measuring $V_a$ (1) across machined slots of increasing length [1]; (2) across a growing fatigue crack, where the length at each measurement point is marked on the fracture surface by a change in applied load;[3] or (3) across a growing fatigue crack in thin specimens where the length is monitored by surface observation [9,10]. An alternative procedure is to use an electrical analog of the test piece [1,23], where the

[1] Engineer, Northern Research and Engineering Corp., Cambridge, Mass. 02139; formerly, undergraduate student, Massachusetts Institute of Technology, Cambridge, Mass.
[2] Associate professor, Department of Mechanical Engineering, Massachusetts Institute of Technology, Cambridge, Mass. 02139. Member of ASTM.

[3] R. O. Ritchie and V. A. Chang, "Calibration of the Electrical Potential Method for W.O.L. Fracture Test Pieces," unpublished research, Rockwell International Science Center, Thousand Oaks, Calif., July 1977.

© 1979 by the American Society for Testing and Materials

Copyright by ASTM Int'l (all rights reserved); Fri Apr 24 19:06:38 EDT 2015
Downloaded/printed by
www.astm.org
Bristol University (Bristol University) pursuant to License Agreement. No further reproductions authorized.

specimen design is duplicated, usually with increased scaled dimensions for better accuracy, using thin aluminum foil [8] or graphitized analog paper [24], and where the crack length can be increased merely by cutting with a razor blade. The tedious and often inaccurate nature of such experimental calibrations, particularly at very short crack lengths [24], has prompted several authors to attempt theoretical solutions to Eq 1. Analytical solutions using conformal mapping procedures have been obtained for several *simple* geometries, namely center and edge-cracked plates with various starter notch or crack configurations [5,6,9, 24]. For more complex geometries such as the compact tension (CT) specimen, however, conformal mapping techniques are not readily applicable, and correspondingly numerical solutions using finite element procedures have been employed [25]. The advantages of theoretical calibrations are several: (1) they are far more accurate at short crack lengths [24,25], (2) they are flexible with regard to varying notch configuration and acuity [24], and (3) they provide a quick and convenient way to select current input and potential measurement probe locations for optimum performance.

The object of the present work is to use recently developed finite element calibration procedures [25] to optimize the electrical potential technique for the widely used compact test piece. That has been attempted qualitatively before by one of the authors through the use of analog patterns [23]. The present studies provide quantitative confirmation and reveal an alternative current input configuration. Further, theoretical calibration curves are computed for selected configurations and are verified by experiment.

## Procedures

### Optimization Analysis

The analysis presented was performed for the metric equivalent of the standard 1-in.-thick (1T) compact test piece (length to width ratio $H/W = 0.6$), currently in widespread use for fracture toughness and subcritical crack growth studies (Fig. 1). Optimization of the electrical potential method for this geometry involves determining the best location for current input and potential measurement leads. Four parameters are considered: accuracy, sensitivity, reproducibility, and what will be referred to as "measurability," as summarized in Table 1.

Accuracy is defined in terms of the degree to which the calibration curve approximates the real relationship between potential change and crack length. For the purposes of this work, this parameter may only be assessed by comparison with experimental and previously obtained theoretical calibrations. However, it must be borne in mind that, in practice, the accuracy of the electrical potential technique may be limited by several other factors, such as the electrical stability and resolution of the potential measurement system, crack front curvature, electrical contact between crack surfaces where the fracture morphology is particularly rough or where significant crack closure effects are present, and changes in electrical resistivity with plastic deformation, temperature variations, or both [1,18].

Sensitivity is defined as the ability of the method to discriminate between small differences in crack length, as illustrated by the slope of the calibration curve $V_a/V_{a0}$ versus $a/W$. Increased resolution may be achieved by maximizing the calibration curve

TABLE 1—*Summary of optimization parameters.*

| Parameter | Limiting Consideration | Mathematical Statement |
|---|---|---|
| Accuracy | accuracy of calibration curve | . . . |
| Sensitivity | slope of calibration curve | maximize $dV/da$ |
| Reproducibility | ability to locate potential leads | minimize $dV/dx$, $dV/dy$ |
| Measurability | magnitude of output voltage signal | maximize $|V_a|$ |
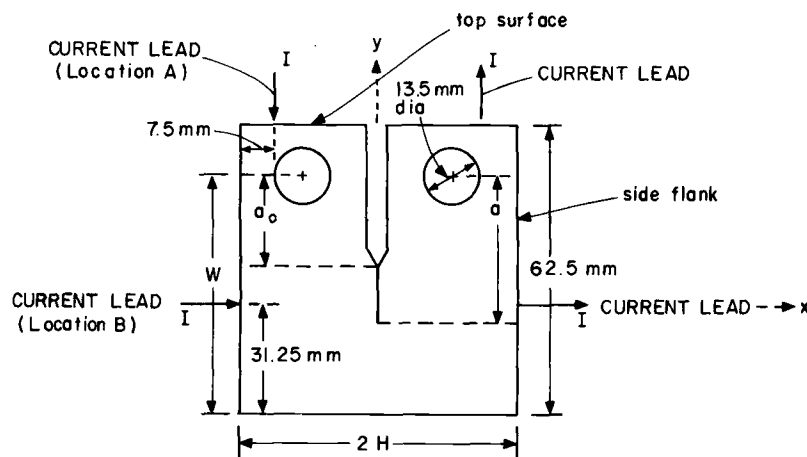


Initial Crack Length $a_0 = 17.5$ mm, Width W = 50mm, 2 H=60mm

FIG. 1—*Geometry of the CT test piece* (H/W = 0.6), *showing selected current* (I) *input Positions A and B.*

slope, and for a particular geometry this is a function of lead placement.

Reproducibility refers to inaccuracies produced by small errors in positioning the potential measurement leads. Such leads are generally fine wires that are spot-welded or screwed to the specimen, and accurate positioning is typically no better than within 0.5 mm. To maximize reproducibility, these leads should be placed in an area where the calibration curve is relatively insensitive to small changes in position, that is, where $dV/dx$ and $dV/dy$ are small, where $x$ and $y$ are position coordinates, with the origin at the midpoint of the specimen, as defined in Fig. 1. This consideration is often at variance with sensitivity considerations, as illustrated by previous results for single-edge-notch geometries [23].

Measurability is defined as the ability of the output voltage signal to be measured over background noise, such as thermal emf, instrument drift and white noise, and so forth. To optimize measurability, current input and potential measurement lead locations are chosen to maximize the absolute magnitude of the output voltage signal $|V_a|$. Since, because of the high electrical conductivity of metals, output voltages are generally at the microvolt level, a practical means of achieving this is simply to increase the input current. However, there is a limit to this increase because when the current is too large (typically exceeding 30 A in a 12.7-mm-thick 1T steel compact test piece), appreciable specimen heating can result from contact resistance at current input positions. Such practical considerations on the use of the potential method are outside the scope of this paper and are documented in detail elsewhere [1].

For purposes of this investigation two current input positions, A and B, previously identified by electrical analog studies, were examined (Fig. 1). Location A involved point introduction of the current on the top surface (sometimes referred to as the notched edge) of the test piece at a distance of 7.5 mm from the side edge. This had previously been regarded as the optimum location [23]. For Location B, current was introduced on the side flanks at a point equidistant from the top and bottom surfaces of the specimen. Potential measurement lead position was then examined for these two current input locations for optimum crack length monitoring. The configurations studied all involved lead placement on the edges of the test piece (top surface and side flanks) because accurate positioning there is more readily obtainable [1]. This is because equipotential surfaces are constant through the thickness of the test piece (except very close to the current input), and thus lead positioning is only a function of one dimension.

*The Finite Element Model*

Finite element analysis as applied to the solution of potential field problems involves the solution of Eq 1 through a variational formulation [25]. If $k$ is the electrical conductivity of the material, $V(x, y)$ is the potential field for the given geometry (assumed here to be two-dimensional), $v$ is the control volume, $S$ is the surface that bounds $v$, and $V_s$ and $i_s$ are the voltages and currents that are specified at the boundary, the variational form of Eq 1 becomes [26,27]

$$\pi = \int_v \tfrac{1}{2}k \left[ \frac{\partial^2 V}{\partial x^2} + \frac{\partial^2 V}{\partial y^2} \right] dv - \int_s V_s i_s \, dS \qquad (2)$$

where $\pi$ is a functional defined so that Eq 1 is obtained when "stationarity" is invoked (that is, the first variation of $\pi$ is set to zero),

$$\delta \pi = 0 \qquad (3)$$

Equations 2 and 3 are solved by dividing the test piece geometry under consideration into a large number of finite elements and by using interpolation to determine the potential at each node. An effective solution is obtained by using variable-number-nodes "isoparametric" elements in which for an element [22],

$$x = \sum_{i=1}^{N} h_i x_i$$

$$y = \sum_{i=1}^{N} h_i y_i$$

and

$$V = \sum_{i=1}^{N} h_i V_i \qquad (4)$$

where $x_i$ and $y_i$ are the spatial coordinates of nodal point $i$, $V_i$ and $h_i$ are, respectively, the electrical potential and relevant interpolation function for node $i$, and $N$ is the number of nodes in the element considered. By substitution of Eq 4 into Eq 2 for all elements of the geometry and by invoking Eq 3, the problem is reduced to the solution of the matrix equation

$$\mathbf{K} \cdot \mathbf{V} = \mathbf{Q} \qquad (5)$$

where $\mathbf{K}$ is the system conductivity matrix, $\mathbf{V}$ is the matrix of potentials at each node, and $\mathbf{Q}$ is the forcing vector that results from the boundary conditions. Solution of Eq 5 is straightforward by linear alegebraic techniques and is well suited to computer implementation [25].

In this study, the computer program ADINAT, developed by Bathe [27], was employed. The specimen was modeled as a two-dimensional figure in the $x$-$y$ plane (thickness assumed constant), symmetrical about the $y$ axis. For increased precision a finer mesh, shown in Fig. 2, was employed than that used previously [25]. Points along the axis of symmetry were assigned zero voltage, except for those in the region of the crack; crack growth was simulated by changing the number of points grounded. Six-node elements were used along the $y$ axis, allowing the coordinate of the middle node of each element (and hence, crack length) to be adjustable at will. Elements near the crack tip, test piece edges, and current input/potential measurement probe locations were finer to obtain improved accuracy.

*Experimental Calibration*

Confirmation of numerical results was achieved by deriving relevant experimental calibration curves for the CT specimen. Measurements were taken of $V_a$ in a 12.7-mm-thick 1T-CT test piece of high strength steel (AISI 4340), where $a$ was increased by cyclic loading. A constant stabilized d-c current was passed

CURRENT INPUT A

|←18 ELEMENT LAYERS →|

16 ELEMENT LAYERS

6 ELEMENT LAYERS

CURRENT INPUT B

5 ELEMENT LAYERS

7 ELEMENT LAYERS

15 ELEMENT LAYERS

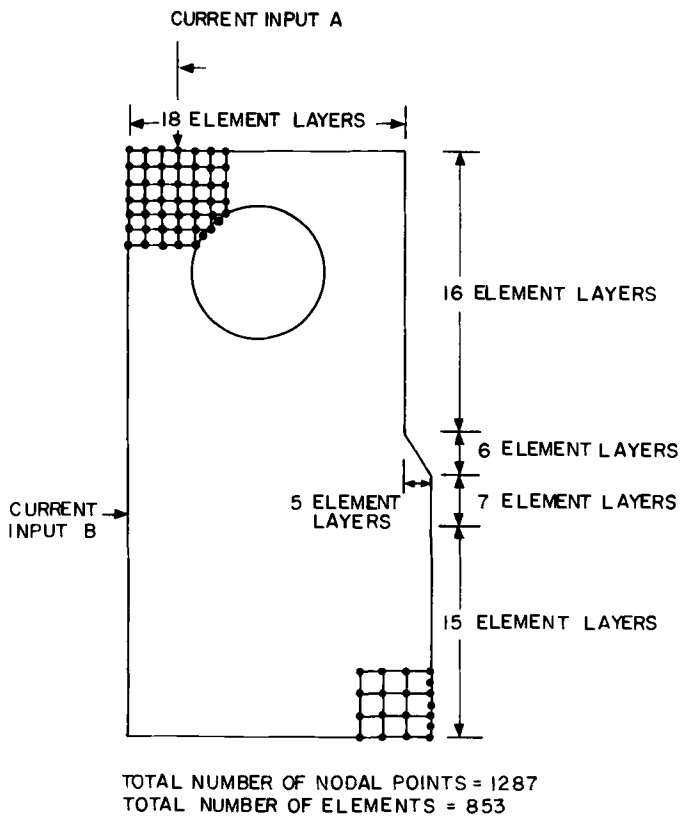TOTAL NUMBER OF NODAL POINTS = 1287
TOTAL NUMBER OF ELEMENTS = 853

FIG. 2—*Finite element idealization of CT specimen.*

through the specimen, which was maintained at constant ambient temperature. The reference potential $V_{a0}$ was measured across the initial notch $a = a_0$ prior to fatiguing. Crack lengths at which potential readings were taken were marked on the fracture surface

by changing the mean load, with the alternating stress intensity $\Delta K$ remaining approximately constant at 20 MPa·m$^{1/2}$. By this procedure sharply defined bands that could be easily measured optically were visible on the fracture surface.

### Results

#### Current Input Location A

The computational results for current input Location A, where the current is introduced at the top surface of the test piece 7.5 mm from the side edge (Fig. 1), are shown in Figs. 3 and 4. This location, together with potential measurement leads placed on the same surface 5.2 mm apart equidistant from the notch centerline (that is, $x = 2.6$ mm), represents the optimum configuration suggested by earlier analog studies [23] and will be referred to as the standard configuration. In the present work the effect of varying potential measurement leads on the top surface from the centerline ($x = 0$) to the edge of the test piece ($x \simeq 29$ mm) was examined. The resultant proportional increase in voltage $V_a/V_{a0}$ as a function of potential lead position $x$ is shown in Fig. 3 for five different crack lengths ($0.4 \le a/W \le 0.68$). Note that the curves are flattest (that is, $dV/dx$ is a minimum) when potential leads are attached close to the notch ($x < 4$ mm), confirming that the standard location of $x = 2.6$ mm yields excellent reproducibility of measurement. For example, for the case of a 2.5-mm crack emanating from the notch ($a/W = 0.4$), an error in lead placement of 5 mm results in a voltage error of less than 5%. As the potential leads are moved further apart ($x$ increasing), the potential error from lead misplacement substantially increases. Similarly, maximum apparent sensitivity (that is, maximum increase in $V_a/V_{a0}$ with increasing $a/W$) is achieved when the potential leads are close to the notch; $V_a/V_{a0}$ decreases markedly, particularly at longer crack lengths, as they are moved further apart. Thus, from both reproducibility
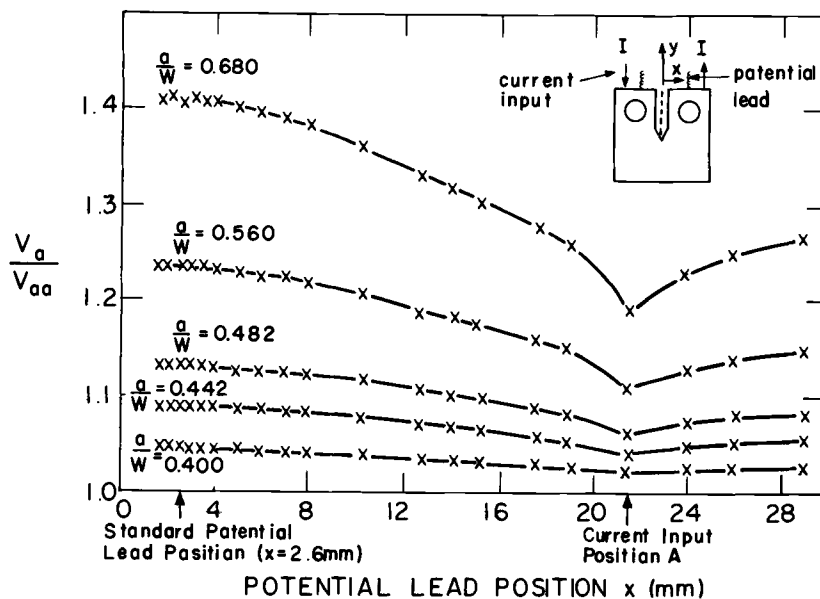
$\dfrac{V_a}{V_{aa}}$

$\dfrac{a}{W} = 0.680$

$\dfrac{a}{W} = 0.560$

$\dfrac{a}{W} = 0.482$

$\dfrac{a}{W} = 0.442$

$\dfrac{a}{W} = 0.400$

current input

potential lead

Standard Potential Lead Position (x=2.6mm)

Current Input Position A

POTENTIAL LEAD POSITION x (mm)

FIG. 3—*Variation of* $V_a/V_{a0}$ *with potential lead Position x on top surface of specimen for current* (I) *input location* A.
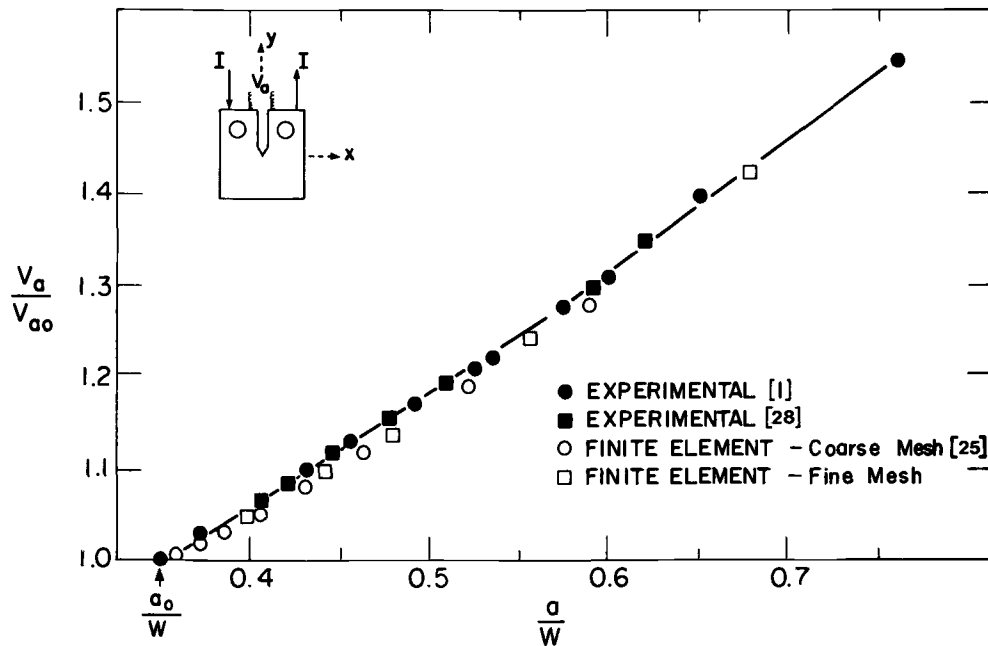
FIG. 4—*Calibration curve for standard configuration of current* (I) *input location* A *with potential leads 2.6 mm equidistant from notch on top surface* (x = 2.6 mm).

and sensitivity considerations, the standard configuration of current input Location A with potential measurement probes attached close to the notch on the top surface (at $x = 2.6$ mm) represents optimum positioning. The calibration curve, in terms of $V_a/V_{a0}$ versus $a/W$ for this configuration, is shown in Fig. 4. Accuracy may be assessed by the fact that the presently computed curve compares very closely to previously determined experimental [1,28] and finite element (employing a coarser mesh) [25] calibrations.

## Current Input Location B

For current Location B, where the current is introduced at the midpoint of the side flank of the test piece (Fig. 1), the effect of varying the potential measurement leads along both the side flank (varying $y$) and the top surface (varying $x$) were investigated. Computational results for the first of these cases are shown in Figs. 5 and 6. With regard to the influence of potential lead position $y$ on $V_a/V_{a0}$, it is apparent from Fig. 5 that reproducibility $dV/dy$ and apparent sensitivity are increased, particularly at longer crack lengths, as the potential leads are moved further from the current input position towards the ends of the specimen (that is, increasing $|y|$). However, although the increase in $V_a/V_{a0}$ per unit increase in $a/W$ (at a potential lead position of, say, $y = 12$ mm) appears somewhat increased with respect to the previously described standard configuration, there is no location for potential leads on this side flank where the curves are flat enough (low $dV/dy$) to guarantee sufficient reproducibility for long cracks. A calibration curve, for potential leads at $y = 13.25$ mm, was derived (Fig. 6) indicating the improved sensitivity (compare Fig. 6 with Fig. 4), but this configuration is not recommended because of potential reproducibility errors.

Far better results with current Location B were obtained by positioning the potential leads on the top surface (varying $x$), as illustrated in Figs. 7 and 8. By moving the potential leads closer
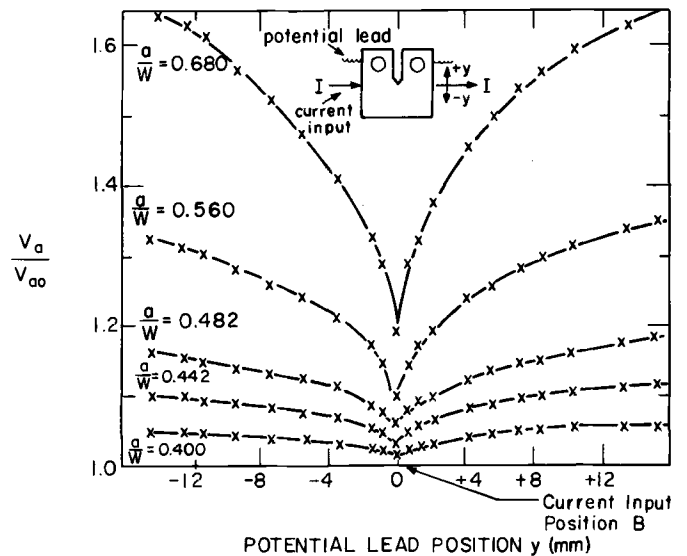


FIG. 5—*Variation of* $V_a/V_{a0}$ *with potential lead position* y *on side flank of specimen for current* (I) *input location* B.

to the notch (decreasing $x$), not only is the proportional increase in voltage $V_a/V_{a0}$ maximized but the curves also become essentially flat ($dV/dx$ minimum for $x \le 4$ mm), insuring good reproducibility, as shown in Fig. 7. As before, this is particularly relevant at longer crack lengths. An optimum potential lead position, then, may be selected close to the notch at, say, $x = 2.6$ mm, identical to that used in the standard configuration with current input location A. The calibration curve of $V_a/V_{a0}$ versus $a/W$ for this configuration was computed and the accuracy confirmed by experimental measurements (Fig. 8). It is clear from this plot that the slope of the calibration curve is distinctly
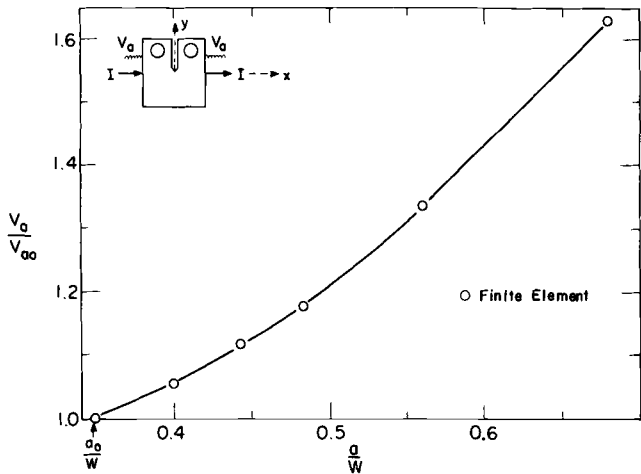
FIG. 6—*Theoretical calibration curve for configuration of current* (I) *input location* B *with potential leads on side flanks of specimen* (y = 13.25 mm).
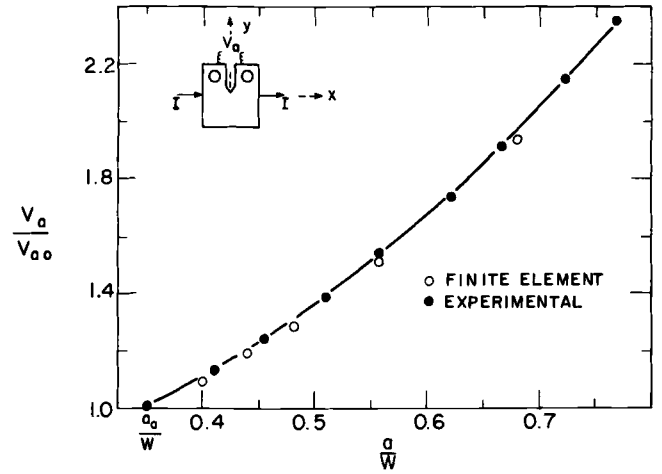


FIG. 8—*Calibration curve for configuration of current* (I) *input location* B *with potential leads 2.6 mm equidistant from notch on top surface* (x = 2.6 mm).
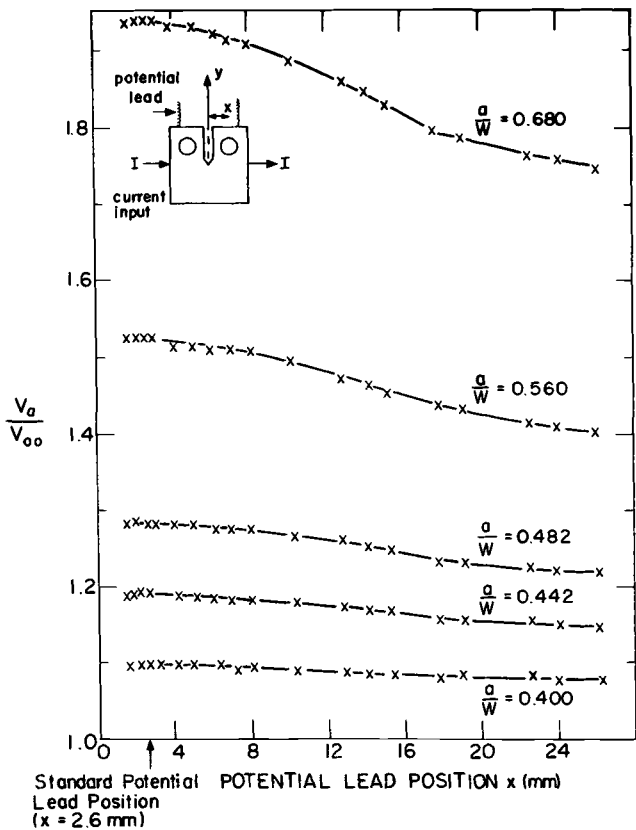
able units, the magnitudes of the output voltage ($|V_a|$) given by the finite element program were roughly 60% smaller for this configuration compared to those for the standard case. This was confirmed by experimental measurements. The low values of these magnitudes, in fact, artificially inflates the value of the ratio $V_a/V_{a0}$ and in reality the actual potential increase per unit increase in crack length is somewhat similar for both configurations, as shown in Fig. 9. A summary and comparison of sensitivity, measurability, and reproducibility considerations for the three configurations examined are also shown in that figure.
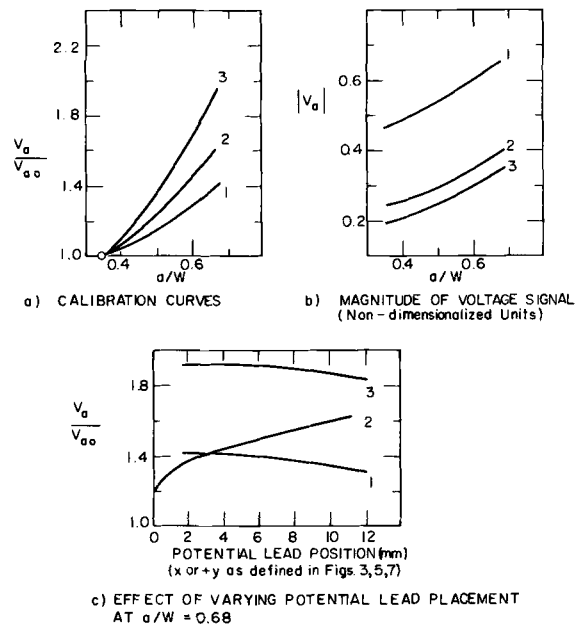


FIG. 7—*Variation of* $V_a/V_{a0}$ *with potential lead position* x *on top surface of specimen for current* (I) *input location* B.



a) CALIBRATION CURVES

b) MAGNITUDE OF VOLTAGE SIGNAL
(Non-dimensionalized Units)

c) EFFECT OF VARYING POTENTIAL LEAD PLACEMENT AT a/W = 0.68

Configurations:   1 - Current Location A, Potential Leads on Top Surface at x = 2.6mm

2 - Current Location B, Potential Leads on Side Flank at y = 13.25mm.

3 - Current Location B, Potential Leads on Top Surface at x = 2.6mm.

FIG. 9—*Summary and comparison of results for the three configurations examined.*

steeper than for the previous two configurations; specifically, by growing a crack from $a/W = 0.35$ to 0.80 the proportional increase in voltage $V_a/V_{a0}$ rises to approximately 2.4 compared to a mere 1.5 for the standard configuration. Based on this and the reproducibility considerations, this configuration of lead placement appears superior to the others investigated. The "measurability," however, was questionable. Though not given in identifi-

## Discussion

The present work has involved the use of finite element analysis to optimize the electrical potential technique for the standard compact test piece by examining the effect of various configurations of current input and potential measurement lead positions. The theoretical calibration curves derived and their close correspondence with experimental measurements indicate the usefulness of such numerical procedures for providing a quick, accurate, and relatively inexpensive means of calibrating complex test geometries that would otherwise require tedious experimental calibration. Moreover, such experimental calibrations would be far less accurate at short crack lengths [24,25].

With regard to lead placement, several points are worthy of note. First, although not explicitly examined in this work, positioning the potential measurement leads close to the precrack tip on the test piece side face will ensure maximum sensitivity and large output voltages, thus allowing much smaller input currents to be used [1]. Despite these obvious advantages, that location is not favored because of the very steep potential gradients there which make this particular configuration highly susceptible to potential reproducibility errors from minor lead misplacement. Second, attaching potential leads in close proximity to current input locations in all cases results in small increases in $V_a/V_{a0}$ with increasing crack length, and large variations in $V_a/V_{a0}$ with minor changes in position, again because of very steep potential gradients (see Figs. 3 and 5). Thus, from apparent sensitivity and reproducibility considerations, the practice of measuring the potential at the point of current input should be avoided. Third, attaching potential leads on the side flanks of the test piece is not recommended because resulting potential measurements are likely to be subject to large errors from lead misplacement (see Fig. 5).

The preferred region for positioning such potential leads appears to be on the top surface as close to the notch as possible (within 4 mm of the notch centerline) because small positional variations produce negligible changes in potential and the proportional increase in voltage $(V_a/V_{a0})$ is maximized there. Selection of current input location, though, for this potential lead position is a matter of choice. The apparent sensitivity, in terms of the increase in $V_a/V_{a0}$ with increasing crack length, is significantly larger with the current introduced at the midpoint of the side flanks (Fig. 9a), yet the absolute magnitude of the voltage output signal $V_a$ is substantially lower ($\sim 60\%$) compared to introducing the current on the top surface (Fig. 9b). Clearly this would be a problem where the technique is to be used for crack monitoring in low resistivity metals, such as aluminum, and thus in this case the standard configuration of both current input and potential measurement lead placement on the top surface of the test piece must be regarded as optimum.

## Conclusion

Finite element analysis has been used to calibrate the electrical potential crack monitoring technique for the standard compact test piece and to optimize the efficiency of the method with regard to this specimen geometry. The numerical solutions derived compare closely with experimental and previously determined theoretical calibrations. Based on considerations of accuracy, sensitivity, reproducibility, and measurability, recommendations

are made for the optimum configurations of current input and potential measurement lead locations.

**References**

[1] Ritchie, R. O., "Crack Growth Monitoring: Some Considerations on the Electrical Potential Method," Departmental Report, Department of Metallurgy and Materials Science, University of Cambridge, England, Jan. 1972.

[2] Trost, A., "Ermittlung von Rissen and Messung der Risstiefen in metallischen Werkstoffen durch elektrische Spannungsmessung," *Metallwirtschaft,* Vol. 23, 1944, pp. 308-309.

[3] Gille, G., "Die Potentialsondenmethode und ihre Anwendung auf die zerstörungsfreie Prüfung grosser Werstücke," *Maschinenschaden,* Vol. 29, 1956, pp. 123-127.

[4] Barnett, W. J. and Troiano, A. R., "Crack Propagation in the Hydrogen-Induced Brittle Fracture of Steel," *Transactions of the AIME,* Vol. 209, No. 4, April 1957, pp. 486-494.

[5] Carlsson, A. J., "Experimental Studies of Fracture Propagation," *Transactions of the Royal Institute of Technology, Stockholm, Sweden,* No. 189, 1962, pp. 1-55.

[6] Gilbey, D. M. and Pearson, S., "Measurement of the Length of a Central Crack or Edge Crack in a Sheet of Metal by an Electrical Resistance Method," Technical Report 66402, Royal Aircraft Establishment, Farnborough, U.K., Dec. 1966.

[7] Steigerwald, E. A. and Hanna, G. T., "Initiation of Slow Crack Propagation in High Strength Materials," *Proceedings,* Vol. 62, American Society for Testing and Materials, Philadelphia, 1962, pp. 885-913.

[8] Anctil, A. A., Kula, E. B., and DiCesare, E., "Electrical Potential Technique for Determining Slow Crack Growth," *Proceedings,* Vol. 63, American Society for Testing and Materials, Philadelphia, 1963, pp. 799-808.

[9] Johnson, H. H., "Calibrating the Electrical Potential Method for Studying Slow Crack Growth," *Materials Research and Standards,* Vol. 5, No. 9, Sept. 1965, pp. 442-445.

[10] Li, C. Y. and Wei, R. P., "Calibrating the Electrical Potential Method for Studying Slow Crack Growth," *Materials Research and Standards,* Vol. 6, No. 8, Aug. 1966, pp. 392-394.

[11] Srawley, J. E. and Brown, W. F., "Fracture Toughness Testing Methods," in *Fracture Toughness Testing and Its Applications, STP 381,* American Society for Testing and Materials, Philadelphia, 1965, pp. 133-196.

[12] Brown, W. F. and Srawley, J. E., *Plane Strain Crack Toughness Testing of High Strength Metallic Materials, STP 410,* American Society for Testing and Materials, Philadelphia, 1967.

[13] Chipperfield, C. G., "Detection and Toughness Characterization of Ductile Crack Initiation in 316 Stainless Steel," *International Journal of Fracture,* Vol. 12, No. 6, Dec. 1976, pp. 873-886.

[14] Jack, A. R. and Price, A. T., "The Initiation of Fatigue Cracks from Notches in Mild Steel Plates," *International Journal of Fracture,* Vol. 6, No. 4, Dec. 1970, pp. 401-409.

[15] Hancock, G. G. and Johnson, H. H., "Subcritical Crack Growth in AM 350 Steel," *Materials Research and Standards,* Vol. 6, No. 9, Sept. 1966, pp. 431-435.

[16] Wei, R. P., Talda, P. M., and Li, C. Y., "Fatigue-Crack Propagation in Some Ultrahigh-Strength Steels," in *Fatigue Crack Propagation, STP 415,* American Society for Testing and Materials, Philadelphia, 1967, pp. 460-485.

[17] Ritchie, R. O. and Knott, J. F., "Mechanisms of Fatigue Crack Growth in Low Alloy Steel," *Acta Metallurgica,* Vol. 21, No. 5, May 1973, pp. 639-648.

[18] McIntyre, P. and Priest, A. H., "Measurement of Sub-Critical

Flaw Growth in Stress Corrosion, Cyclic Loading and High Temperature Creep by the DC Electrical Resistance Technique," BISRA Open Report No. MG/54/71, British Steel Corporation, London, June 1971.

[19] Johnson, H. H. and Willner, A. M., "Moisture and Stable Crack Growth in a High Strength Steel," *Applied Materials Research,* Vol. 4, No. 1, Jan. 1965, pp. 35-40.

[20] McIntyre, P., "Influence of Environment on Crack Growth in High Strength Steels," *Proceeding of the Conference on The Mechanics and Mechanisms of Crack Growth,* British Steel Corporation, London, 1973, pp. 121-151.

[21] Haigh, J. R., Skelton, R. P., and Richards, C. E., "Oxidation-Assisted Crack Growth During High Cycle Fatigue of a 1% Cr-Mo-V Steel at 550°C," *Materials Science and Engineering,* Vol. 26, No. 2, Dec. 1976, pp. 167-174.

[22] Unangst, K. D., Shih, T. T., and Wei, R. P., "Crack Closure in 2219-T851 Aluminum Alloy," *Engineering Fracture Mechanics,* Vol. 9, No. 3, 1977, pp. 725-734.

[23] Ritchie, R. O., Garrett, G. G., and Knott, J. F., "Crack Growth Monitoring: Optimization of the Electrical Potential Technique Using an Analog Method," *International Journal of Fracture Mechanics,* Vol. 7, No. 4, Dec. 1971, pp. 462-467.

[24] Clark, G. and Knott, J. F., "Measurement of Fatigue Cracks in Notched Specimens by Means of Theoretical Electrical Potential Calibrations," *Journal of Mechanics and Physics of Solids,* Vol. 23, No. 4/5, Aug./Oct., 1975, pp. 265-276.

[25] Ritchie, R. O. and Bathe, K. J., "On the Calibration of the Electrical Potential Technique for Monitoring Crack Growth Using Finite Element Methods," *International Journal of Fracture,* Vol. 15, No. 1, Feb. 1979, pp. 47-55.

[26] Bathe, K. J. and Wilson, E. L., *Numerical Methods in Finite Element Analysis,* Prentice-Hall, Englewood Cliffs, N.J., 1976.

[27] Bathe, K. J., "ADINAT—A Finite Element Program for Automatic Dynamic Incremental Nonlinear Analysis of Temperatures," MIT Acoustics and Vibration Laboratory Report No. 82448-5, Massachusetts Institute of Technology, Cambridge, 1977.

[28] Garrett, G. G., "Toughness and Cyclic Crack Growth Studies in Aluminum Alloys," Ph.D. thesis, University of Cambridge, England, July 1973.